Contribution for the development of a novel connection system between GFRP pultruded profiles

João Pedro Sintra Viegas Sobreiro de Azevedo

Department of Civil Engineering, Architecture and Georesources, Instituto Superior Técnico, Universidade de Lisboa

Abstract: This paper presents the development of a novel beam-to-column bolted connection system between tubular GFRP pultruded profiles. The geometrical properties and material selection for the steel cuff connection system aimed at achieving better performance in terms of stiffness and resistance, and in terms of ductility and energy dissipation capacity. To study the behaviour of this system, full-scale tests were made in two beam-to-column connections with different bolt configurations: W – with one bolt through the beam webs; and F – with two bolts through the beam flanges. The experiments comprised three monotonic tests and three cyclic tests for each configuration. In the monotonic tests, the stiffness, resistance and ductility of the connections were evaluated. In each cycle of the cyclic tests, the evolution of stiffness, resistance and absorbed energy were assesed. The monotonic behaviour of both configurations was numerically modelled using the Abaqus finite element software package, and the damage progression was investigated resorting to Hashin damage model. In this regard, a parametric study of the fracture energies of the GFRP material was performed. Despite some limitations, the numerical models presented reasonable agreement with the experimental data, especially for configuration F. In general, the novel connection system provided good performance in comparison with previous systems.

Keywords: Pultruded GFRP profiles; Beam-to-column connection; Steel cuff connection; Experimental tests; Numerical analysis; Damage progression.

1. Introduction

Fibre reinforced polymer (FRP) composites are made of a fibre reinforcement, typically, glass, aramid or carbon, impregnated in a polymeric matrix. In construction, glass and carbon FRPs are the most commonly used (GFRP and CFRP, respectively) [1], especially GFRP due to their lower production costs. These composites present great potential to civil engineering applications, largely due to their: (i) high resistance; (ii) lightness; (iii) reduced self-weight; (iv) high durability, even in aggressive environments (chemical or physical); and (v) reduced maintenance costs. In contrast, GFRP have relatively low elasticity modulus, orthotropic behaviour and brittle failure.

FRPs can be produced by various methods, pultrusion being the one that presents lower production costs. Through pultrusion, any type of linear parts with constant cross section can be produced. Most sections were copied from steel construction, namely thin-wall sections. Pultruded profiles have most of their fibres oriented in the pultrusion axis, leading to the anisotropic behaviour of the material. This behaviour and the constituent materials lead to characteristic brittle failure modes that should be taken into account in the design process.

Initially, beam-to-column connections between pultruded GFRP profiles were also copied from steel construction. Therefore, those connections (in general, between I-section profiles) consisted of seated GFRP angles bolted to the beam's web and column's flange, and were designed as pinned. Nevertheless, designing GFRP structures with pinned connections can be very penalizing in terms of deformations, leading to inefficient and uneconomical profile selections.

Various connection systems were developed, especially for I-section profiles. These connection systems were deemed to achieve higher rotational stiffness in order to allow the connections to be designed as semi-rigid. However, these systems presented other problems and consequently an efficient way to connect these profiles has not yet been achieved.

This study was driven by the need to develop a novel connection system between GFRP pultruded tubular profiles, which would present considerable ductility and capacity to dissipate energy, without compromising the stiffness and resistance of the connection.

To study the behaviour of this novel connection system, full-scale tests were carried out in beam-to-column connections subjected two different types of loading: (i) monotonic; and (ii) cyclic. Two bolt configurations were tested and three tests have been made for each configuration and type of loading. At the same time, numerical models were developed to simulate the monotonic behaviour of both connection configurations. A parametric study of the GFRP fracture energies was performed based on the comparison between the numerical and experimental results. The agreement between the numerical models and the monotonic tests was assessed in terms of connections' stiffness, strength and damage/failure modes.

2. Literature review

Connections between FRP elements can be either (i) bolted, and/or (ii) bonded. Bonded connections present better compatibility with FRP materials, since stress transfer is more uniform. However, the connections between GFRP

profiles were initially copied from steel construction, generally bolted, resulting in added difficulties, especially due to the high stress concentration near the bolts' holes and the orthotropic behaviour of the material. Thus, most investigation until now consists in single-lap and double-lap tests in plates and were meant to characterize the failure modes of the material (Figure 1). Mottram and Turvey [2] reviewed the work of several authors in order to study the influence of the connections dimensions on the different failure modes, as illustrated in Figure 1.

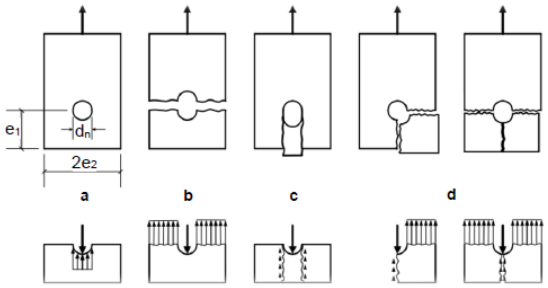

Figure 1: FRP bolted connection failure modes (a – bearing; b – net-tension; c – shear-out; and d – cleavage), adapted from [3].

Xiao and Ishikawa [4, 5] concluded that the only failure mode that presents some failure ductility is the bearing one. Furthermore, Mottram and Turvey [2] concluded that, single-row connections may be designed for bearing failure, this is not the case for multiple row connections. Bank's *Composites for Construction* [6] and the *Eurocomp Design Code and Handbook* [7] provide, respectively, pre-design rules for in-plane connections and for the stress distribution between rows of bolts (which is not uniform as in steel connections, due to the absence of plastic deformations in the material).

Concerning beam-to-column connections, these were initially designed as pinned, for web cleated connections (with two GFRP seated angles placed on the beam's web), and as semi-rigid, in the case of flange cleated connections (with two GFRP seated angles on the beam's flanges) [8]. It is important to note that those connections were made between I-section beams and columns.

Bank *et al.* [9] studied these connections and tried to combine both (Figure 2-a) in order to achieve higher values of stiffness and resistance. Despite their efforts, those connections were still too flexible and failed for moderate loads. Thereafter, a series of improved GFRP angles were created (Bank *et al.* [10]; Mosallam *et al.* [11]; and Bank *et al.* [12], Figure 2-b, c and d respectively) in order to improve the connections between I-section profiles. With these prototypes, improvements in stiffness and resistance were achieved, although each prototype was more difficult to produce, assemble and still presented brittle failure modes. Also, these prototypes presented drawbacks in terms of compatibility with other building elements.

Smith *et al.* [13] identified that most problems were probably related with the use of I-section profiles, having suggested the use of tubular profiles connected with the first prototype of a GFRP cuff (Figure 2-e). The author obtained an increase in stiffness and especially in resistance. Based on this work, Singamsethi *et al.* [14] proposed a new cuff made of GFRP (Figure 2-f), which was later produced and tested by Carrion *et al.* [15], and provided an increase in stiffness and resistance compared with Smith's *et al.* cuff connection.

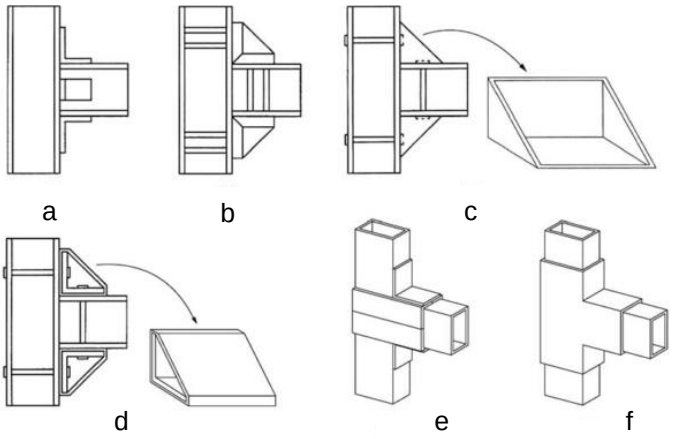

Figure 2: a – Bank *et al.* [9, 10]; b – Bank *et al.* [10]; c – Mosallam *et al.* [11]; d – Bank *et al.* [12]; e – Smith *et al.* [13]; and f – Singamsethi *et al.* [14] and Carrion *et al.* [15]. Adapted from [15].

Qureshi and Mottram [16-18] studied web cleated and flange cleated connections with steel angles, concluding that the use of steel in these connections brings improvements in terms of stiffness. More recently, Proença [19] and Wu *et al.* [20] tested steel sleeve connections (internal to the tubular GFRP profiles), obtaining satisfactory results.

These studies show that the use of tubular profiles together with the use of steel connection pieces might be the way to obtain a more effective method to connect pultruded GFRP profiles. Making use of the entire section of the column also seems to be advantageous in obtaining a better connection performance.

To study GFRP connections numerically, most studies resorted to damage initiation criteria (Hashin, Tsai-Wu and Tsai-Hill are the most used ones). The use of these criteria is essential to identify the damage in the GFRP elements, but does not allow the analysis of the complete behaviour of these connections, since it does not allow evaluating the influence of damage progression. Therefore, the use of damage progression models is necessary. These models can be constant or continuous, the latter being more realistic and the former generally too conservative [21].

Several authors studied beam-to-column connections resorting to numerical models. Casalegno *et al.* [22] studied numerically a GFRP web cleated connection and the connection presented in Figure 2-a. Carrion *et al.* [23] studied numerically their GFRP cuff connection. Zhang *et al.* [24] studied the connection tested by Wu *et al.* [20]. All these studies resorted to 3D finite element models and a damage initiation criterion. However, none of these studies used damage progression models with the exception of the study performed by Casalegno *et al.*, in which a constant damage progression model was used. All the numerical models presented good agreement with the experimental results in terms of stiffness and resistance. The damage in the GFRP was well predicted, but the complete influence of the damage progression was not evaluated.

Proença [19] studied his connections numerically, resorting to the Hashin damage initiation criterion and a continuous damage progression model, based on the

fracture energies of the GFRP material. The author used the fracture energies proposed by Nunes *et al*. [25], and obtained satisfactory results in comparison with the experimental tests, in terms of stiffness, resistance and also of damage progression.

The studies reviewed above show that in order to fully evaluate the behaviour of beam-to-column connections, it is essential to use continuous damage progression models. The main difficulty lies in setting the values for the fracture energies of the GFRP, which are still largely unknown.

3. Experimental study

3.1. Experimental program

The experimental study was performed in the *Laboratório de Estruturas e Resistência dos Materiais* (LERM) of *Instituto Superior Técnico* (IST). This study consisted of testing two bolt configurations for the novel beam-to-column connection. Three monotonic tests and three cyclic tests were performed for each configuration.

The monotonic tests aimed at determining the stiffness, resistance and ductility of each configuration. Meanwhile, the objective of the cyclic tests was to evaluate the evolution of stiffness, resistance and absorbed energy in each cycle. In both types of tests, the damage in the GFRP pultruded members was also assessed.

3.2. Geometrical properties of the joint system

The beam-to-column connection system developed in this study consists of a steel cuff connection, as illustrated in Figure 3. In terms of geometry, this connection is similar to the ones proposed by Smith *et al.* [13] and Sigamsethi *et al.* [14]. With this geometry, the connection was intended to transfer moment not only through the bolts, but also by the contact between the profiles and the cuff, thus reducing the typical damage of bolted GFRP connections. Furthermore, this connection was produced with very thin steel sheeting (2 mm), bent and welded to create the desired geometry. The configuration of the welds is shown in Figure 4 and Figure 5. The point of this very thin steel sheeting was to achieve higher ductility and energy dissipation capacity.

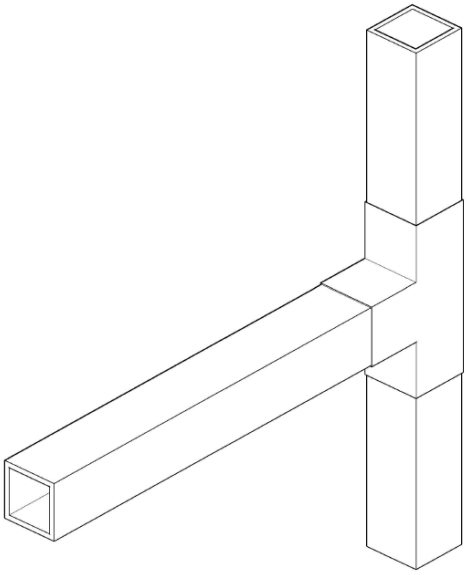

Figure 3: 3D geometry of the novel joint system.

This bolted steel cuff provided the connection between a column with 1080 mm of height and a beam with 960 mm of length, both made of a GFRP pultruded RHS 120x120x10,0 mm^3 cross section. Two bolt configurations were studied: (i) configuration W, with an M12 Cl8.8 bolt through the webs of the beam and two M8 Cl8.8 bolts through the flanges of the column (Figure 4); and (ii) configuration F, with two M12 Cl8.8 bolts through the beam flanges and two M8 Cl8.8 bolts through the column flanges (Figure 5). In the latter configuration, two bolts were used in order to prevent the failure of the connection from occurring due to shear in the bolts. The use of two bolt configurations allowed studying their influence on the behaviour of the connection. It should be noted that configuration F presents worse compatibility with floor panels (because of the bolts' nuts), although it is believed that this difficulty can be easily overcome.

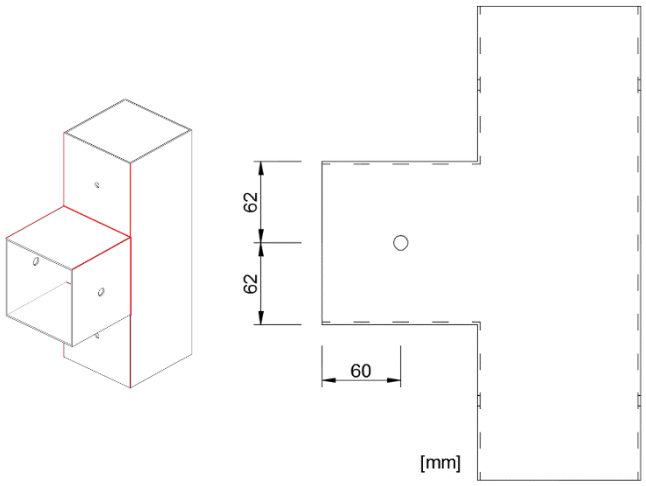

Figure 4: Configuration W (welds in red on the 3D view).

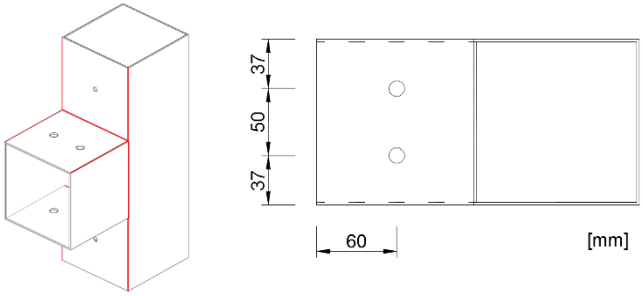

Figure 5: Configuration F (welds in red on the 3D view).

3.3. Setup, instrumentation and procedure

Both monotonic and cyclic tests were performed inside a closed steel frame, using the setup presented in Figure 6. Both column ends were fixed (rotations and displacements prevented) to the steel frame and the torsion of the beam was prevented with two aluminium cylindrical bars (Figure 6).

The load was applied to the beam at a distance of 600 mm from the face of the column flange by an *Enerpac* hydraulic jack, with load capacities of 600 kN and 250 kN, respectively in compression and tension, and a maximum stroke of 250 mm. The applied load was measured by a *TML* load cell with 300 kN of load capacity (both in tension and compression). Ten displacement transducers and two rotation transducers (all from *TML*) were used to measure: (i) the beam's vertical displacements; (ii) the beam's rotation; (iii) the column's rotation, and (iv) the joint's horizontal displacement. The rotation of the beam and column were measured in two distinct ways: with the rotation transducers, measuring the rotations in the steel

cuff; and with pairs of displacement transducers, measuring the rotations in the members (in the beam and, in the column, above and below the cuff). Considering that the measurement of the rotation in the members is the most representative of the overall connection's behaviour, the rotations considered were the ones measured with the displacement transducers.

The monotonic tests were performed by applying a descending vertical load until a displacement of ~135 mm is reached, while the cyclic tests were done with a displacement history defined in accordance with the monotonic tests (with a maximum displacement of ±125 mm, due to the maximum stroke of the hydraulic jack).

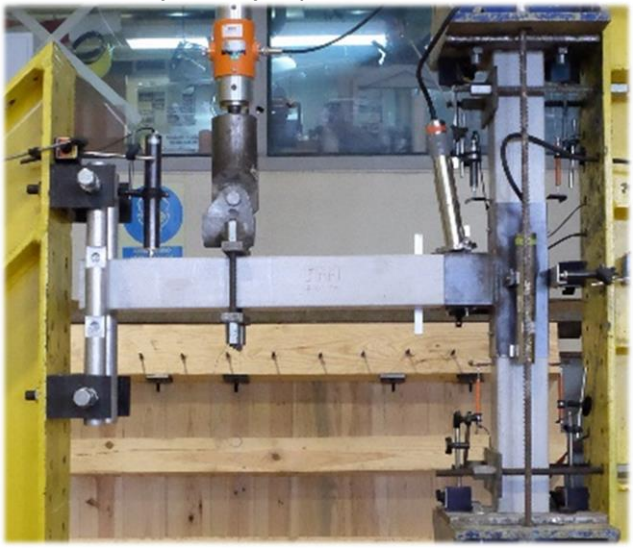

Figure 6: Test setup.

The parameters analysed from the monotonic tests are illustrated in Figure 7. In addition, the rotational stiffness (K_Φ) was obtained from the moment-rotation curve in the same way as the deformation stiffness (K_δ).

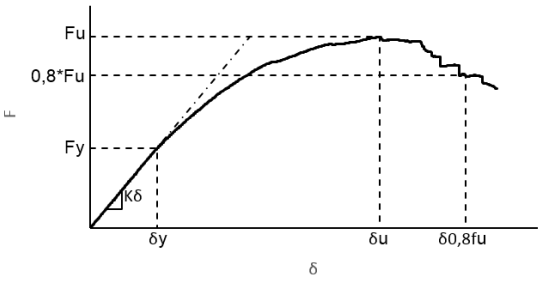

Figure 7: Parameters analysed from the monotonic tests.

The displacement $\delta_{0,8fu}$ was considered to study the ductility of the connection; it corresponds to one of the relative ductility definitions (Equation 1) proposed by Stehn and Björnfot [26] (cited by Jorissen and Fragiacomo [27]) for steel-to-timber connections.

$$C_d = \frac{\delta_{0,8fu} - \delta_y}{\delta_{0,8fu}} \quad (1)$$

3.4. Results and discussion

3.4.1. Monotonic tests

As mentioned before, three monotonic (M) tests were performed in each configuration for a total of six tested specimens (WM1, WM2, WM3, FM1, FM2 and FM3). All tests were considered valid. Figure 8 and Figure 9 present, respectively, the load *vs.* vertical displacement curves obtained for configuration W and configuration F. Both configurations initially displayed a linear behaviour. For average displacements of ~21 mm for configuration W and ~27 mm for configuration F, the connections started to exhibit non-linear behaviour with stiffness reduction. All specimens reached failure afterwards, followed by a reduction of the load, which was gradual in some specimens and sudden in others. The only exception was specimen WM3 that never reached failure (the hydraulic jack reached its maximum stroke).

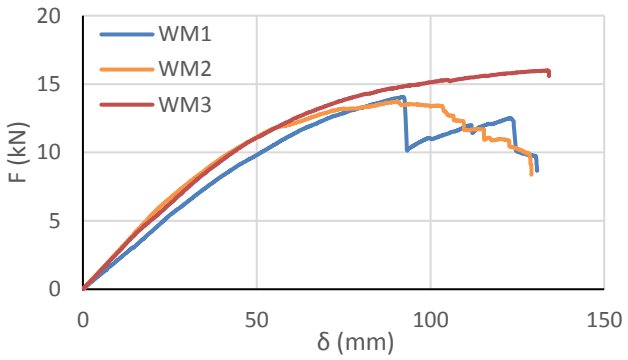

Figure 8: Load *vs.* vertical displacement of configuration W.

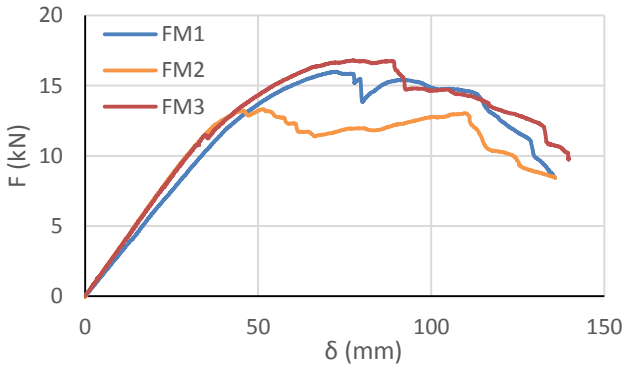

Figure 9: Load *vs.* vertical displacement of configuration F.

The damage in both configurations was assessed during the tests and after the disassembly of the specimens.

The main damage modes in configuration W were: (i) bearing, sometimes followed by shear out, on the web bolt holes of the GFRP beam (Figure 10); (ii) web-flange junction failure of the GFRP beam (typically responsible for the failure of the connections, Figure 10); and (iii) significant yielding of the steel cuff.

Configuration F presented the following damage modes: (i) bearing sometimes followed by shear out on the top flange bolt holes of the GFRP beam (Figure 11); (ii) web-flange junction failure on the GFRP column; and (iii) failure of the weld that connects the webs of the column and the beam in the steel cuff (typically responsible for the failure of the connections, Figure 12).

Table 1 presents the main values measured in the monotonic tests. In general, configuration F presented better performance than configuration W, with higher values of stiffness (K_δ and K_Φ) and "yield" load (F_y). In terms of resistance and ductility, both configurations presented similar values.

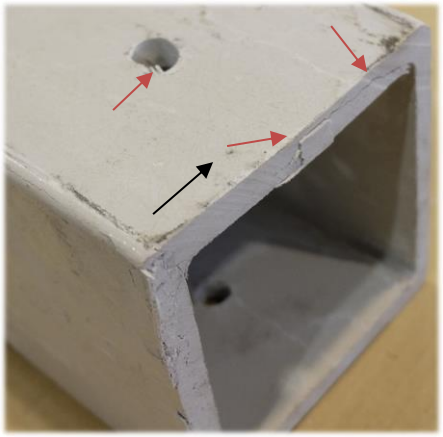

Figure 10: WM1 GFRP beam damage.

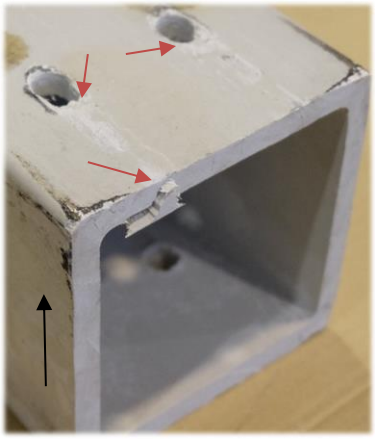

Figure 11: FM3 GFRP beam damage.

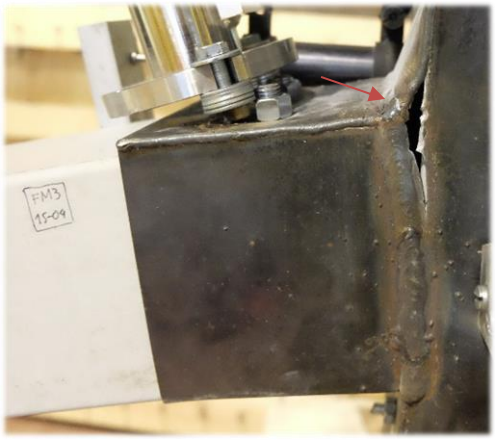

Figure 12: FM3 steel cuff failure.

Table 1: Results of the monotonic tests.

Configuration	K_δ	K_φ	F_y	F_u	δ_y	δ_{fu}	$C_{d,\delta}$
	kN/m	kN.m/rad	kN	kN	mm	mm	-
W	252,0±33,4	99,3±13,9	5,3±0,53	14,6±1,23	21,4±3,54	105,4±24,4	0,81±0,07
F	330,8±25,8	138,9±17,7	8,7±0,82	15,4±1,82	26,6±4,72	67,1±14,0	0,77±0,04

Considering an elastic analysis (more suitable for GFRP structures) and a beam with 3000 mm of span, it is possible to define both configurations as semi-rigid in accordance with Eurocode 3. This defines the connections, for this type of analysis, as a function of the beam's stiffness. Figure 13 illustrates the comparison between the stiffness of both configurations and the limits for fixed and pinned connections.

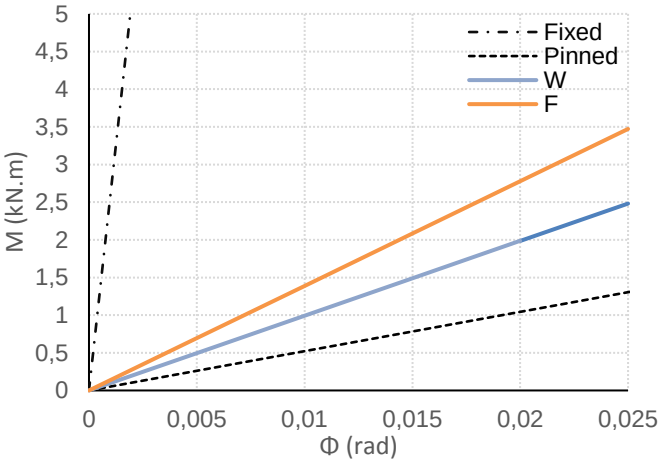

Figure 13: Comparison between the rotational stiffness of both configurations and limits defined by Eurocode 3.

3.4.2. Cyclic tests

The cyclic tests were performed in accordance with ECCS' *Recommended testing procedure for assessing the behaviour of structural steel elements under cyclic loads* [28]. Therefore, two displacement histories were defined, one for each configuration, based on their "yield" displacements (21 mm and 27 mm respectively for configurations W and F). Table 2 presents these displacement histories.

As mentioned before, three cyclic (C) tests were performed for each configuration, resulting in a total of six tested specimens (WC1, WC2, WC3, FC1, FC2 and FC3). All tests were considered valid, with the exception of the test of specimen WC3, which was not valid due to a defect on the steel cuff.

Table 2: Displacement histories as per ECCS [28].

Cycle	ECCS	δ (W)	δ (F)
	[-]	[mm]	[mm]
1st	[δy/4; -δy/4]	[5,25; -5,25]	[6,75; -6,75]
2nd	[δy/2; -δy/2]	[10,5; -10,5]	[13,5; -13,5]
3rd	[3δy/4; -3δy/4]	[15,75; -15,75]	[20,25; -20,25]
4th	[δy; -δy]	[21; -21]	[27; -27]
5th	[2δy; -2δy]	[42; -42]	[54; -54]
6th	[2δy; -2δy]	[42; -42]	[54; -54]
7th	[2δy; -2δy]	[42; -42]	[54; -54]
8th	[4δy; -4δy]	[84; -84]	[108; -108]
9th	[4δy; -4δy]	[84; -84]	[108; -108]
10th	[4δy; -4δy]	[84; -84]	[108; -108]
11th	[6δy; -6δy]	[126; -126]	-
12th	[6δy; -6δy]	[126; -126]	-
13th	[6δy; -6δy]	[126; -126]	-

Figure 14 and Figure 15 present examples of the load *vs.* vertical displacement curves measured in the cyclic tests for both configurations, comparing also the most representative curves from the monotonic tests for the respective configuration.

For both configurations, the hysteretic curves presented reasonable symmetry, although this symmetry was lost in configuration F, due to the damage of the steel cuff. Both configurations presented a baseline where the connection did not absorb any load. This baseline was caused by a small clearance in the steel cuff and became larger with the cycles due to the damage progression.

The damage modes were similar to the ones observed in the monotonic tests for both configurations. Additionally, configuration W also presented (i) failure of the weld responsible for the web-flange junction in the steel cuff, (ii) buckling of the beam's webs and (iii) crushing of the

beam's corners. Configuration F also presented (i) failure of the weld responsible for the web-flange junction in the steel cuff, and (ii) failure of the weld responsible for the connection between the webs of the beam and the webs of the column in the steel cuff, which occurred not only in the top part of the weld, but also at the bottom part, with those damages eventually merging for larger displacements.

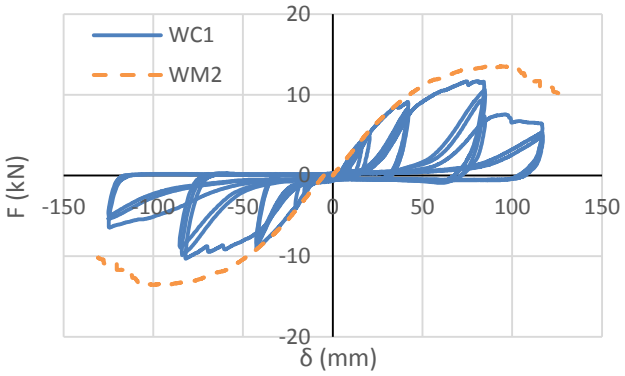

Figure 14: Cyclic test of specimen WC1.

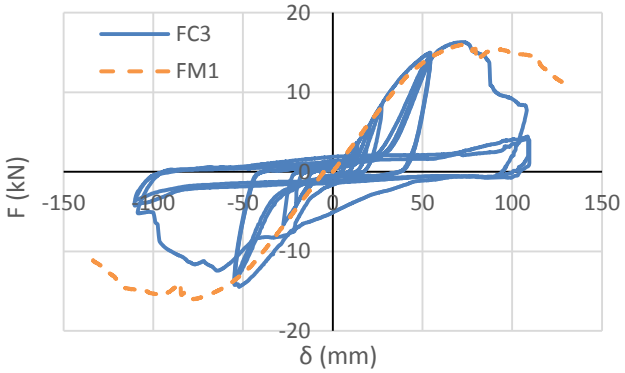

Figure 15: Cyclic test of specimen FC3.

Table 3 presents the average maximum and minimum loads for each configuration and their respective displacements. Generally, configuration F presented higher loads. Nevertheless, those occurred for smaller displacements, which is consistent with the higher stiffness of this configuration.

Table 3: Average maximum and minimum loads and respective displacements for each configuration.

Configuration		F_{max} (kN)	F_{min} (kN)	δ_{max} (mm)	δ_{min} (mm)
W	Average	14,06	-12,20	100,84	-82,95
	Std-dev	3,30	2,65	28,24	1,23
F	Average	16,22	-15,79	79,20	-54,37
	Std-dev	0,15	1,88	8,86	2,94

Figure 16 presents the average resistance ratios per cycle for both configurations. Both configurations presented an ascending tendency until the 5th cycle, in which the "yield" displacement was surpassed. The resistance ratios dropped in the repetitions of the same displacement and rose once more when the displacement was again increased (8th cycle). Thereafter, the resistance dropped in every cycle, for both configurations.

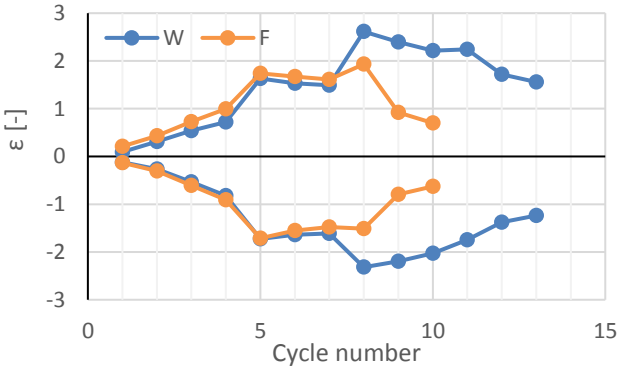

Figure 16: Average resistance ratios per cycle.

Figure 17 presents the average stiffness ratios per cycle for both configurations. Neither configuration showed a clear tendency throughout the cyclic tests. This may be due to the fact that the stiffness was measured on the unloading stage of each cycle in the intersection with the abscissa axis, in which the transition to the aforementioned baseline occurred.

Figure 18 presents the average absorbed energy ratios per cycle, for both configurations. As it was expected, each increase of the displacement (after "yield") presented an increase in the absorbed energy ratio, which was reduced on load repetitions for the same displacement.

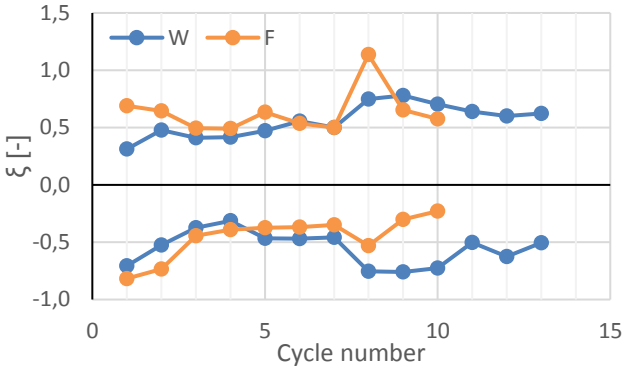

Figure 17: Average stiffness ratios per cycle.

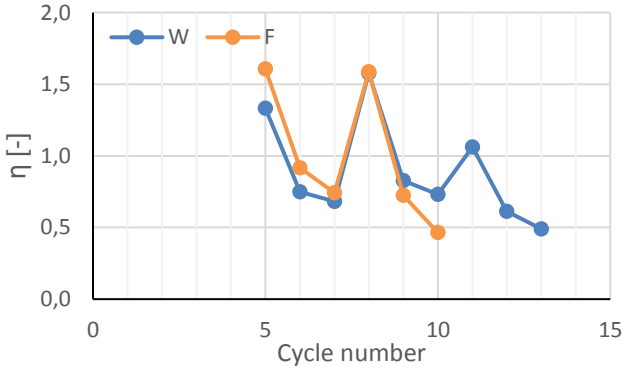

Figure 18: Average absorbed energy ratios per cycle.

Figure 19 presents the average accumulated absorbed energy for both configurations. Configuration F absorbed significantly more energy than configuration W, showing that, despite the moment transfer of the connection relying mostly on the contact between the profiles and the cuff, the bolted configurations also influenced the behaviour of the connection.

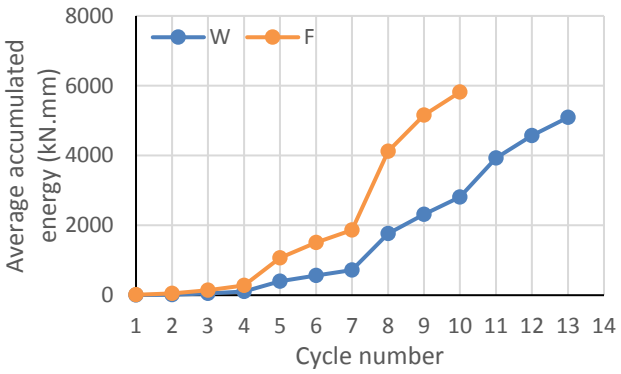

Figure 19: Average accumulated absorbed energy.

In conclusion, generally, configuration F presented better performance for cyclic loading.

4. Numerical analysis

4.1. Model description

The numerical analysis presented here was made resorting to Abaqus 6.13 [29] finite element (FE) commercial software.

4.1.1. Geometry, mesh and discretization

All the geometrical properties of the modelled connection were carefully simulated in accordance to the specimens tested. Since the connection was symmetrical, only half of it was modelled.

The GFRP members were modelled using two different types of FEs: (i) continuum shell (SC8R) elements in the connection area and next to it; and (ii) frame (B33) elements, in the regions farther away from the connection. The steel cuff was modelled with continuum shell (SC8R) elements and the bolts with tetrahedral solid elements (C3D4). Table 4 presents the properties of the mesh used, which was the most refined from three different discretizations tested.

Table 4: Mesh properties.

Structural element	Type of element	Number of elements
Column	Frame (B33)	5
	Continuum Shell (SC8R)	936
Beam	Frame (B33)	12
	Continuum Shell (SC8R)	7876
Cuff	Continuum Shell (SC8R)	4555
M8 bolts	Solid (C3D4)	592
M12 bolts	Solid (C3D4)	4945

4.1.2. Material properties

The GFRP was modelled as orthotropic and using the Hashin and Rotem [30] damage model, based on the fracture energies of the material. Both, the failure criterion and the degradation model are conveniently explained by Nunes *et al.* [31]. The Hashin criterion considers six failure modes, in tension (T), compression (C) and shear (S), in the longitudinal (1) and transverse (2) directions. The elastic properties of the GFRP are presented in Table 5 and the resistances are listed in Table 6. All these properties were obtained from the work of Proença [19], who performed experimental tests to determine the material properties, with the exception of the $f_{1,S}$ value, which was determined from double-lap tests in an ongoing study at IST. The fracture energies used are addressed in section 4.2.

Table 5: GFRP elastic properties.

E_{11} [GPa]	E_{22} [GPa]	υ_{12} [-]	$G_{12}=G_{13}=G_{23}$ [GPa]
32,7	4,8	0,3	3,2

Table 6: GFRP resistant properties.

$f_{1,T}$ [MPa]	$f_{1,C}$ [MPa]	$f_{2,T} = f_{2,C}$ [MPa]	$f_{1,S}$ [MPa]	$f_{1,S}$ [MPa]
326	435	89	30	59

The properties of the steel sheeting (S235), listed in Table 7, were determined in the present study through tensile tests.

Table 7: Steel sheeting mechanical properties.

E [GPa]	υ [-]	σ_y [MPa]	σ_u [MPa]	$\varepsilon_{u,pl}$ [-]
189,45	0,3	260	350	0,24

The steel bolts were modelled in accordance with Eurocode 3 with a modulus of elasticity of 195 GPa, an yield stress of 640 MPa and an ultimate stress of 800 MPa.

4.1.3. Boundary conditions

Figure 20 displays the boundary conditions of the numerical model of configuration W, as an example. The load was applied at a distance of 600 mm of the column's facing flange and consisted of a 120 mm imposed displacement. Both column ends were fixed (displacements and rotations restrained) and all the faces coincident with the symmetry plane were modelled with a longitudinal sliding boundary condition, so the symmetry simplification was valid.

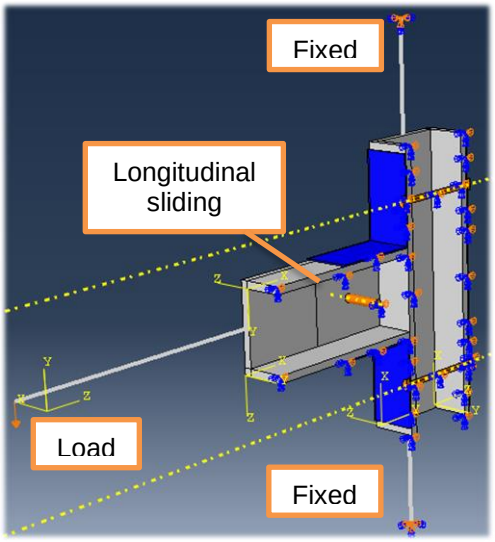

Figure 20: Boundary conditions (W).

4.1.4. Contact and friction formulation

All contacts were modelled as frictionless and with a stiffness of 10000 MPa/mm, sufficiently rigid to discard their effect on the connection stiffness. The only exception was the contact between the top flanges of the GFRP beam and the cuff, which was modelled with a numerical artificial clearance of 1 mm (to simulate the actual clearance of the steel cuff). Because this clearance

brought convergence problems, the stiffness of this contact was changed to 5000 MPa/mm. Surface-to-surface contact and small-sliding theory were used in all surfaces.

4.1.5. Type of analysis

The analysis performed in the numerical models was static implicit (standard), geometrically linear and physically non-linear (for all materials). The analysis was conducted through an imposed vertical displacement, at the point of the applied load. The Newton-Raphson method was used.

4.2. Fracture energy parametric study

Although there are some values reported in the literature about the fracture energy of FRP materials [25, 32-35], most of the studies refer to carbon-epoxy composites and present significant variability. Furthermore, none of the values were obtained from experimental tests.

Due to the uncertainty about these values a parametric study was done. This study included three phases summarized in Table 8, in which the fracture energies are for fibres in compression ($G_{f,C}$), fibres in tension ($G_{f,T}$), matrix in compression ($G_{m,C}$) and matrix in tension ($G_{m,T}$).

In the first phase, all combinations of those values were tested. In that phase, a good agreement was always obtained between experimental and numerical results for configuration F, while for configuration W such agreement was worse due to the premature failure caused by the matrix damage in tension, in the beam's webs. In both configurations, the fracture energy of the fibres in tension presented no influence whatsoever in the results, but for some values convergence problems were encountered. This seems to have been caused by the use of the numerical artificial clearance in the contact between the top flanges of the beam and the steel cuff. These problems increased after the occurrence of damage and were more significant in connection W for $G_{m,C}$=50 N/mm.

Table 8: Fracture energy values tested in the parametric study.

Phase	$G_{f,C}$ [N/mm]	$G_{f,T}$ [N/mm]	$G_{m,C}$ [N/mm]	$G_{m,T}$ [N/mm]
1st	5	200 100 50 25 15	5 10 25 50	70
2nd	5	50	25	100 125 150
3rd	5	50	75	150
			100	150
			150	200

Therefore, in the second phase, the values of $G_{f,T}$ and $G_{m,C}$ were fixed in the combination that presented better agreement for both configurations and the values of $G_{m,T}$ were increased. The numerical results for configuration F continued to present good agreement with the experimental ones, but the convergence problems increased. For configuration W, the damage of the matrix in tension was reduced, although the damage of the matrix in compression increased and, consequently, this configuration continued to present a premature failure.

Finally, in the third phase, both matrix fracture energies were increased, and the combinations presented in Table 8 were used. Configuration F maintained the same behaviour in all phases. This was due to the fact that the behaviour of this configuration was mostly ruled by the steel yielding. The resistance of configuration W increased (compared to the previous phase) and failure was less premature, although the numerical results still presented significant differences the experimental ones. All fracture energy combinations led to convergence problems for configuration F and the last combination presented the same problems for configuration W. As such, the chosen combination was the one presented in Table 9.

Table 9: Chosen fracture energies combination.

$G_{f,C}$ [N/mm]	$G_{f,T}$ [N/mm]	$G_{m,C}$ [N/mm]	$G_{m,T}$ [N/mm]
5	50	100	150

4.3. Results and discussion

The following section presents the results obtained with the FE models for both configurations, only for the final phase of the numerical study. To evaluate the global damage in the GFRP material the DAMAGESHR variable was used, since this variable includes all damage modes (fibres and matrix, in tension and compression) and the PEEQ variable was used to evaluate the yielding distribution of the steel cuff.

Figure 21 and Figure 22 present the load *vs.* vertical displacement obtained with the numerical models of the monotonic tests, for configurations W and F, respectively. The curves of both configurations initially present two distinct linear branches with different values of stiffness. In the first one (with stiffness $K_{\delta 1}$) the contact between the top flanges of the GFRP beam and the steel cuff was not yet established, so the moment transfer was only due to binary in the bolts. After damage occurred (bearing of the GFRP near the holes), contact was established, allowing the moment transfer to happen not only through the bolts, but also by contact with the steel cuff (with stiffness $K_{\delta 2}$). For both configurations, this was followed by a gradual loss of stiffness. Finally, configuration W reached the failure load (F_u), for which the connection experiences a sudden load drop; configuration F did not present such a behaviour, displaying an elastoplastic response. This occurred because the cuff's steel was modelled as elastoplastic, without softening, and the failure of this configuration occurred in the steel.

The higher initial stiffness of the models compared to that measured in the experiments was studied in further depth. It was concluded that the relative difference in stiffness should be due to the degradation of the GFRP material near the hole, due to the bearing of the GFRP caused by the bolts' threads. Yet, one decided to not include this effect in the models, since identifying the full extent of this degradation, or quantifying it precisely would not be possible within the present study.

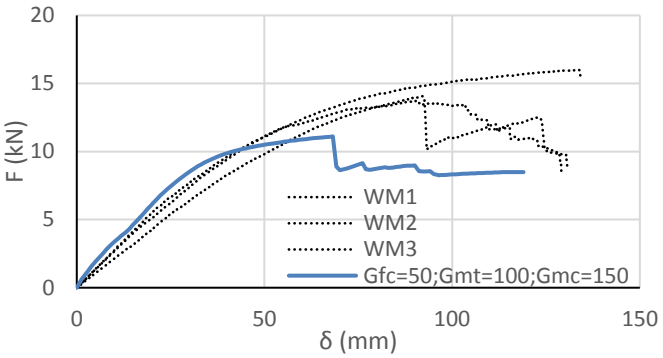

Figure 21: Load *vs.* vertical displacement for configuration W.

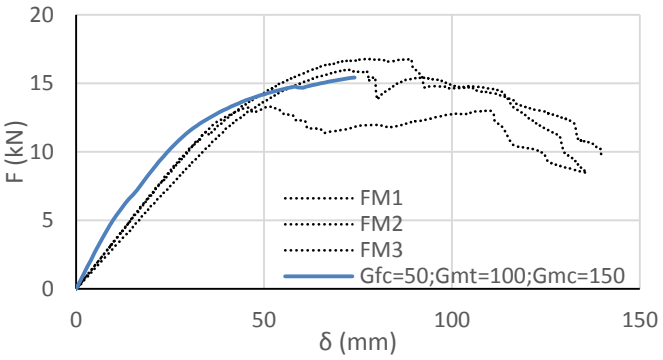

Figure 22: Load *vs.* vertical displacement for configuration F.

Table 10 presents the comparison between the numerical and experimental results corresponding to the monotonic tests, Δ being the relative difference. In terms of stiffness, initially the numerical results were considerably higher than the experimental ones, but after the contact of the top flanges was established, the values of stiffness presented good agreement (less than 25% of relative difference). Concerning the connection resistance, for configuration W the numerical value was lower than the experimental one due to the aforementioned premature damage in the beam's webs, while for configuration F a good agreement was obtained (in this configuration the numerical resistance considered corresponded to the maximum load attained, since the model was leaning towards a constant load value).

Table 10: Comparison between numerical and experimental results.

	Parameter	W	F
Experimental	K_δ [kN/m]	252,0 ± 13,6%	330,8 ± 7,8%
	F_u [kN]	14,6 ±8,4%	15,4 ± 11,8%
Numerical	K_δ [kN/m]	471,2	558,9
	Δ [%]	+87,0	+69.0
	K_δ [kN/m]	297,5	335.6
	Δ [%]	+18,1	+1.5
	F_u [kN]	11,1	15.4
	Δ [%]	-23,9	+0.4

Figure 23 presents the damage distribution in the GFRP for both configurations. The numerical model of configuration W (Figure 23-a) provided a similar damage pattern to that observed experimentally, with a crack in the web-flange junction and another one aligned with the hole. This is similar to the experimental damage, which generally occurred in the web-flange junction, sometimes extending adjacently to the hole (Figure 10). The bearing on the hole was also predicted, but without evolving to shear-out. The numerical model of configuration F (Figure 23-b) predicted the bearing on the holes of the beam's top flange, without developing to shear-out either (Figure 11), and also the damage in the web-flange junction of the column. These results are consistent with the ones observed experimentally, since the shear-out of the bolts did not always occur.

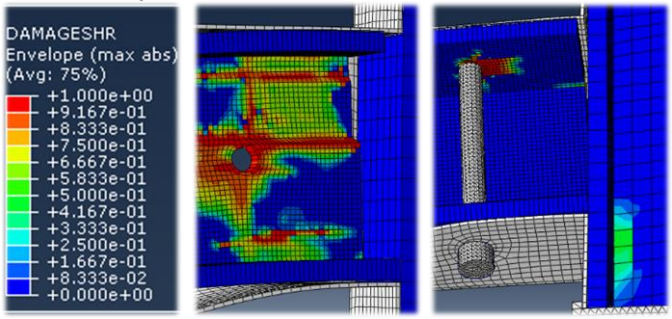

a b

Figure 23: DAMAGESHR in both models. a – W and b – F.

Figure 24 presents the yielding of both connections. For connection W (Figure 24-a) the model presented good results, since the most plasticized part of the steel cuff is consistent with that observed in the experimental tests. For connection F (Figure 24-b) the results were also compatible with the experiments, since the most plasticized part of the steel cuff was the one in which failure was seen to occur in the experiments (Figure 12).

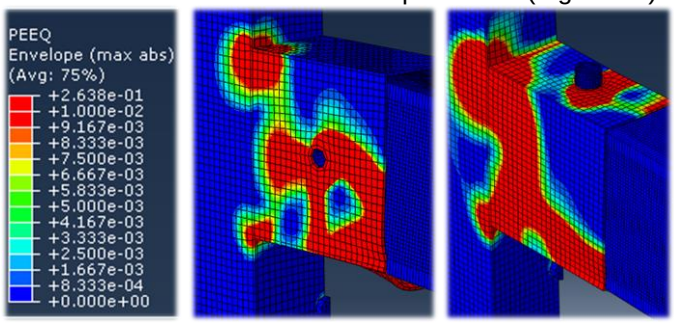

a b

Figure 24: PEEQ in both models. a – W and b – F.

5. Conclusions

In the present study, a novel beam-to-column connection system was developed, which was proved to offer advantages over the existing systems. In fact, the system developed presents a good balance between structural performance, ease of assembly and fabrication, and compatibility with other building elements.

The tests on the beam-to-column connections allowed assessing the behaviour of two alternative bolt configurations. In terms of serviceability behaviour to monotonic loads, configuration F presented higher values of stiffness and "yield" load. Nevertheless, both configurations presented similar values of failure load and ductility. Concerning the cyclic behaviour, configuration F also provided better performance, presenting higher values of dissipated energy. Regarding the damage progression, for both types of load (monotonic and cyclic),

the two bolt configurations presented significant damage in the GFRP profiles (especially the beam), with configuration F presenting more extensive yielding and damage in the steel cuff. Since the steel cuff was produced with a very thin steel sheeting (2 mm), it should be noted that the only construction limitations come from the bolt nuts' position. In this aspect, configuration W presents advantages when compared to configuration F, although the limitations of the latter can be easily overcome.

Comparing the monotonic behaviour of this novel connection system with the one studied by Proença [19], it is possible to conclude that significant improvements were achieved. Table 11 presents a comparison of the results in terms of rotational stiffness (K_Φ), "yield" load (F_y) and failure load (F_u), Δ being the relative difference between the highest values obtained here for configuration F (which provided better results). It should be noted that these values can be compared because the load was applied at the same distance from the joint and the columns and beams had the same dimensions.

Table 11: Configuration F vs. Proenças' sleeves.

Connection system	K_Φ (kN.m/rad)	F_y (kN)	F_u (kN)
Proença's Sleeves	106,0	4,70	8,73
Steel cuff (F)	138,9	8,67	15,37
Δ	+31,0 %	+84,5 %	+76,1 %

Regarding the numerical study of the monotonic behaviour of the connections, despite the generally good agreement between the numerical and experimental results, some limitations were identified. It was confirmed that, ideally, the simulation of this kind of structural problems should be conducted resorting to not only to the damage initiation criteria of the materials involved, especially the GFRP, but also to the damage progression. Only in this way is it possible to evaluate precisely the behaviour of the connections, since the use of damage initiation criteria alone does not allow studying their full behaviour.

Studies of beam-to-column connection systems with finite element models resorting to continuous damage progression models are still quite scarce. In this study, which aimed at implementing these models, it was concluded that the major difficulty is the determination of the GFRP fracture energies. Therefore, a parametric study of the GFRP fracture energies was made, in which a combination that provided satisfactory results was achieved.

Due to the complex geometry of this connection system, some problems were identified in obtaining values of stiffness similar to those obtained in the experimental tests. Nevertheless, with the simulation of the cuff clearance, and after the contact was established, the values of stiffness obtained from the models were quite similar to the experimental ones. Additionally, it was concluded that the reason for the higher initial stiffness in the models must have been the local degradation/bearing of the GFRP material near the hole caused by the bolt threads.

The resistance predicted for the configuration F was in good agreement with the experiments, as this model presented a behaviour similar to an elastoplastic one, in which the resistance tended to stabilize for values similar to the experimental ones. This was due to the fact that the behaviour of this connection was essentially ruled by the yielding of the steel cuff instead of the GFRP damage. As the steel softening was not modelled, it was not possible to predict a failure load (in the tests, the failure of this configuration was caused by rupture of the cuff's steel). In what refers to configuration W, the numerical model had the tendency to present a premature failure in the webs of the GFRP beam, considerably underestimating its resistance. It is likely that this difference was due to the uncertainty in the fracture energies and, possibly due to the fact that continuum shell elements were used, which just have one element throughout the entire thickness of the section walls. Despite all this, overall the damage/failure modes were well predicted by the numerical model.

References

[1] A. M. Girão Coelho and J. T. Mottram, "A review of the behaviour and analysis of bolted connections and joints in pultruded fibre reinforced polymers", Mater. Des., vol. 74, pp. 86–107, 2015.

[2] J. T. Mottram and G. J. Turvey, "Physical test data for the appraisal of design procedures for bolted joints in pultruded FRP structural shapes and systems", Prog. Struct. Eng. Mater., vol. 5, no. 4, pp. 195–222, 2003.

[3] J. T. Mottram, "Design guidance for bolted connections in structures of pultruded shapes: gaps in knowledge", Seventeenth Int. Conf. Compos. Mater., 2009.

[4] Y. Xiao and T. Ishikawa, "Bearing strength and failure behavior of bolted composite joints. Part I: Experimental investigation", Compos. Sci. Technol., vol. 65, no. 7–8, pp. 1022–1031, 2005.

[5] Y. Xiao and T. Ishikawa, "Bearing strength and failure behavior of bolted composite joints. Part II: Experimental investigation", Compos. Sci. Technol., vol. 65, no. 7–8, pp. 1032–1043, 2005.

[6] L. C. Bank, Composites for Construction. Hoboken, New Jersey: John Wiley & Sons, Inc., 2006.

[7] Clarke JL, Structural Design of Polymer Composites – EUROCOMP Design Code and Handbook. London: E.&F.N. Spon, 1996.

[8] J. T. Mottram and Y. Zheng, "State-of-the-art review on the design of beam- to-column connections for pultruded frames", Compos. Struct., vol. 35, no. 4, pp. 387–401, 1997.

[9] L. C. Bank, A. S. Mosallam, and H. E. Gonsior, "Beam-to-column connections for pultruded FRP structures", in Serviceability and Durability of Construction Materials, 1990, pp. 804–813.

[10] L. C. Bank, a. S. Mosallam, and G. T. McCoy, "Design and performance of connections for pultruded frame structures", J. Reinf. Plast. Compos., vol. 13, no. 3, pp. 199–212, 1994.

[11] A. S. Mosallam, M. K. Abdelhamid, and J. H. Conway, "Performance of pultruded FRP connections under static

and dynamic loads", J. Reinf. Plast. Compos., vol. 13, no. 5, pp. 386–407, 1994.

[12] L. C. Bank, J. Yin, L. Moore, D. J. Evans, and R. W. Allison, "Structures, experimental and numerical evaluation of beam-to-column connections for pultruded", J. Reinf. Plast. Compos., vol. 15, no. 10, pp. 1052–1067, 1996.

[13] S. J. Smith, I. D. Parsons, and K. D. Hjelmstad, "An experimental study of the behaviour of connection for pultruded GFRP- I beams and rectangular tubes", Compos. Struct., vol. 42, no. 3, pp. 281–290, 1998.

[14] S. K. Singamsethi, J. M. LaFave, and K. D. Hjelmstad, "Fabrication and testing of cuff connections for GFRP box sections", Compos. Constr., vol. 9, no. 6, pp. 536–544, 2005.

[15] J. E. Carrion, J. M. LaFave, and K. D. Hjelmstad, "Experimental behavior of monolithic composite cuff connections for fiber reinforced plastic box sections", Compos. Struct., vol. 67, no. 3, pp. 333–345, 2005.

[16] J. Qureshi and J. T. Mottram, "Moment-rotation response of nominally pinned beam-to-column joints for frames of pultruded fibre reinforced polymer", Constr. Build. Mater., vol. 77, pp. 396–403, 2015.

[17] J. Qureshi and J. T. Mottram, "Behaviour of pultruded beam-to-column joints using steel web cleats", Thin-Walled Struct., vol. 73, pp. 48–56, 2013.

[18] J. Qureshi and J. T. Mottram, "Response of beam-to-column web cleated joints for FRP pultruded members", Journal Compos. Constr., vol. 18, no. 2, pp. 1–11, 2014.

[19] M. Proença, "Behaviour of bolted connections between GFRP composite profiles", Master Dissertation in Civil Engineering (in Portuguese), Instituto Superior Técnico, 2015.

[20] C. Wu, Z. Zhang, and Y. Bai, "Connections of tubular GFRP wall studs to steel beams for building construction", Compos. Part B Eng., no. 95, pp. 64–75, 2016.

[21] C. Hühne, A. K. Zerbst, G. Kuhlmann, C. Steenbock, and R. Rolfes, "Progressive damage analysis of composite bolted joints with liquid shim layers using constant and continuous degradation models", Compos. Struct., vol. 92, no. 2, pp. 189–200, 2010.

[22] C. Casalegno, A. Picariello, and S. Russo, "Analysis of all-GFRP beam-column bolted joints through progressive failure approach", Compos. Struct., vol. 33, no. 2, pp. 81–87, 2012.

[23] J. E. Carrion, K. D. Hjelmstad, and J. M. LaFave, "Finite element study of composite cuff connections for pultruded box sections", Compos. Struct., vol. 70, no. 2, pp. 153–169, 2005.

[24] Z. Zhang, C. Wu, X. Nie, Y. Bai, and L. Zhu, "Bonded sleeve connections for joining tubular GFRP beam to steel member: Numerical investigation with experimental validation", Compos. Struct., vol. 157, no. 1, pp. 51–61, 2016.

[25] F. Nunes, N. Silvestre, and J. R. Correia, "Structural behaviour of hybrid FRP pultruded columns. Part 2: Numerical study", Compos. Struct., vol. 139, pp. 304–319, 2016.

[26] L. Stehn and A. Björnfot, "Comparison of different ductility measurements for a nailed steel-to-timber connection", in Proceedings of the 7th World Conference on Timber Engineering, 2002.

[27] A. Jorissen and M. Fragiacomo, "General notes on ductility in timber structures", Eng. Struct., vol. 33, no. 11, pp. 2987–2997, 2011.

[28] ECCS, Recommended Testing Procedure for Assessing the Behaviour of Structural Steel Elements under Cyclic Loads (no 45). Brussels: ECCS, 1986.

[29] Simulia, Abaqus 6.13 User's Manual. 2013.

[30] Z. Hashin and A. Rotem, "A fatigue criterion for fiber-reinforced materials", J. Compos. Mater., vol. 7, pp. 448–464, 1973.

[31] F. F. Nunes, "Comportamento estrutural de perfis pultrudidos de GFRP reforçados com mantas de CFRP Caracterização experimental e modelação numérica", 2012.

[32] E. J. Barbero, F. A. Cosso, R. Roman, and T. L. Weadon, "Determination of material parameters for Abaqus progressive damage analysis of E-glass epoxy laminates", Compos. Part B Eng., vol. 46, pp. 211–220, 2013.

[33] A. M. Girão Coelho, J. Toby Mottram, and K. A. Harries, "Finite element guidelines for simulation of fibre-tension dominated failures in composite materials validated by case studies", Compos. Struct., vol. 126, pp. 299–313, 2015.

[34] P. Maimí, P. P. Camanho, J. A. Mayugo, and C. G. Dávila, "A continuum damage model for composite laminates: Part II – Computational implementation and validation", Mech. Mater., vol. 39, no. 10, pp. 909–919, 2007.

[35] S. T. Pinho, P. Robinson, and L. Iannucci, "Fracture toughness of the tensile and compressive fibre failure modes in laminated composites", Compos. Sci. Technol., vol. 66, no. 13, pp. 2069–2079, 2006.